PCCP

Accepted Manuscript

This article can be cited before page numbers have been issued, to do this please use: S. Canola, C. Graham, Á. J. J. Pérez-Jiménez, J. Sancho-Garcia and F. Negri, *Phys. Chem. Chem. Phys.*, 2018, DOI: 10.1039/C8CP06727A.

This is an Accepted Manuscript, which has been through the Royal Society of Chemistry peer review process and has been accepted for publication.

Accepted Manuscripts are published online shortly after acceptance, before technical editing, formatting and proof reading. Using this free service, authors can make their results available to the community, in citable form, before we publish the edited article. We will replace this Accepted Manuscript with the edited and formatted Advance Article as soon as it is available.

You can find more information about Accepted Manuscripts in the author guidelines.

Please note that technical editing may introduce minor changes to the text and/or graphics, which may alter content. The journal's standard Terms & Conditions and the ethical guidelines, outlined in our author and reviewer resource centre, still apply. In no event shall the Royal Society of Chemistry be held responsible for any errors or omissions in this Accepted Manuscript or any consequences arising from the use of any information it contains.

View Article Online
DOI: 10.1039/C8CP06727A

Journal Name

ARTICLE

Charge transport parameters for carbon based nanohoops and donor-acceptor derivatives

Received 00th January 20xx,
Accepted 00th January 20xx

DOI: 10.1039/x0xx00000x

www.rsc.org/

Sofia Canola,[a,b] Christina Graham,[a,c,d] Ángel José Pérez-Jiménez,[c] Juan-Carlos Sancho-García*[c] and Fabrizia Negri*[a,b]

The role of donor-acceptor (D-A) moieties on magnitudes such as reorganization energies and electronic couplings in CycloParaPhenylenes (CPP) carbon based nanohoops (i.e. conjugated organic molecules with cyclic topology) is highlighted via model computations and analysis of the available crystalline structure of N,N-dimethylaza[8]CPP. For the sake of comparison, intra-molecular and inter-molecular charge transport parameters are concomitantly modelled for the recently determined herringbone polymorph of [6]CPP, along with [8]CPP and [12]CPP. The peculiar contribution of low frequency vibrations to intramolecular reorganization energies is also disclosed by computing the Huang-Rhys factors for the investigated [n]CPPs and the N,N-dimethylaza derivative. In contrast with most planar organic semiconductors where the layer in which molecules are herringbone arranged identifies the high-mobility plane, nanohoops disclose inter-layer electronic couplings larger than the intra-layer counterparts. Charge transfer rate constants modelled with three different approaches (Marcus, Marcus-Levich-Jortner and spectral overlap) suggest that D-A nanohoops, owing to orbital localization, may be more efficient for charge transport than [n]CPPs for suitable solid phase arrangements.

Introduction

Aromatic carbon nanorings are fascinating carbon rich structures that possess radially oriented p orbitals and several unique properties.[1-3] Cycloparaphenylenes (CPPs) in particular, are ring-shaped aromatic hydrocarbons consisting exclusively of n units of paraphenylenes. π-extended derivatives of CPPs, incorporating naphthalene rings, cyclo-1,4-naphthylenes (CNs) have also been synthesized.[4] CPPs and related carbon nanorings have been proposed as building blocks for a rational "bottom-up" synthesis of homogeneous armchair carbon nanotubes (CNTs), given that CPPs represent the shortest sidewall segment of armchair CNTs.[5] The strong interest in the bottom-up design of CNTs is culminated, very recently, after several unsuccessful attempts, in the synthesis a true belt segment of (n,n)CNT[6] and even more recently in the extension to larger nanobelt analogues. [7]

The unique properties of nanorings and nanobelts create new opportunities for the application of organic compounds in materials science, [8] for instance an increased solubility compared to linear oligoparaphenylenes.[1,2] Moreover, because of the curved structure and cyclic conjugation, the energy of the HOMOs of [n]CPPs becomes higher than that in linear [n]paraphenylenes. [9-11] Small CPPs have small HOMO-LUMO gaps and it has been shown that oxidation produces stable cationic species. [12-14] Similarly, reduction has been reported indicating that these systems may be used for multielectron storage.[15, 16] Raman spectroscopy has been used to probe the electronic structure changes of [n]CPPs as a function of their sizes/diameters. The pseudo radial breathing mode (p-RBM) and the radial breathing mode (RBM) frequencies have been identified and shown to display a linear dependence on the inverse of the diameter of the ring, in close analogy with CNTs. [17-19]

As regard their condensed phases, most CPPs pack into the typical herringbone pattern of polycyclic aromatic hydrocarbons [20, 21] except for the small [6]CPP that exhibited a tubular-like packing.[2] However very recently a herringbone polymorph of [6]CPP has also been determined. [16]

[a] Dipartimento di Chimica 'G. Ciamician', Università di Bologna, Via F. Selmi 2, 40126 Bologna, Italy.
[b] INSTM, UdR Bologna, Italy.
[c] Department of Physical Chemistry, University of Alicante, 03080 Alicante, Spain.
[d] Institute of Photonic Sciences (ICFO), 08860 Castelldefels (Barcelona), Spain
† Corresponding authors e-mail: fabrizia.negri@unibo.it, jc.sancho@ua.es.

Electronic Supplementary Information (ESI) available: absolute energies, energy of the frontier molecular orbitals, reorganization energies from AP method, intermolecular distances of the dimers considered, parameters employed to compute the rate constants, electronic couplings and rate constants. Molecular structure and comparison among equilibrium structures, frontier molecular orbitals, HR factors and representation of active modes, details on charge transport paths), electronic couplings of the model systems upon translation and rotation. See DOI: 10.1039/x0xx00000x

View Article Online
DOI: 10.1039/C8CP06737A

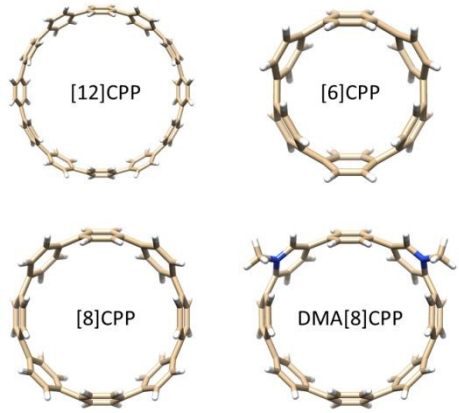

Fig. 1. The molecular nanohoops investigated in this work.

Many optoelectronic organic materials featuring donor–acceptor (D–A) moieties have been extensively investigated and applied in artificial photosynthesis[22] and organic solar cells.[23] The D-A concept applied to fully conjugated macrocycles has led to chiral conjugated corrals [24] and other cyclic structures that have been shown to outperform the acyclic counterparts in organic photovoltaics.[25] Several other D-A nanohoops have been designed starting from CPPs.[26] For example an anthraquinone (AQ) or a tetracyano-anthraquinodimethane (TCAQ) moiety have been inserted into the [10]CPP ring as an acceptor [27]. In addition aza[6]CPP, methylaza[6]CPP[28], aza[8]CPP containing one, two, and three nitrogens and alkylated analogues N-methylaza[8]CPP and N,N-dimethylaza[8]CPP, were prepared and characterized [29] and for the latter the solid state packing has been successfully reported. In all these derivatives the bent phenylene unit is the electron-rich donor.

Alkylation of the nitrogen centre shifts the LUMO energy level to lower energies, leaving the HOMO energy levels essentially unaffected, thereby resulting in a dramatically decreased HOMO–LUMO energy gap. This molecular engineering strategy would lead to D-A nanohoops of potential interest as ambipolar semiconductors, due to the concomitant presence of *p*-type and *n*-type moieties, a strategy previously adopted in the design of other core-extended conjugated organic semiconductors.[30]

Several computational investigations have contributed to get insight on the unique properties of CPPs, covering structural, energetic, electronic, magnetic properties [9,10,17,31,32,33] along with their potential application in optoelectronics[34], for instance as thermally activated delayed fluorescence emitters.[35] In addition, charge transport properties of [n]CPPs were initially explored through the estimate of intramolecular reorganization energies and electronic couplings.[36]

Prompted by the availability of the crystal structure of N,N-dimethylaza[8]CPP (hereafter labelled DMA[8]CPP, see also Fig.1 and Fig. S1) we explore here how electronic couplings may be tuned in D-A systems, via arrangement in the solid phase, and compare them with those of [n]CPPs (n=6,8,12). Owing to the recent availability of the herringbone polymorph of [6]CPP [16] we investigate the charge transport parameters of this and two additional nanohoops also arranging in a similar crystal structure: [8]CPP and [12]CPP. Because the approach adopted in a previous study [36] might have overestimated electronic couplings, and for a cost-effective quantitative comparison between all the molecules tackled here, we use a fragment orbital protocol tested for several different organic semiconductors in previous investigations.[37-43] Besides inter-molecular electronic couplings, the vibrational modes assisting charge transport via contribution to intra-molecular reorganization energies are determined and compared to those usually active for planar core organic semiconductors.

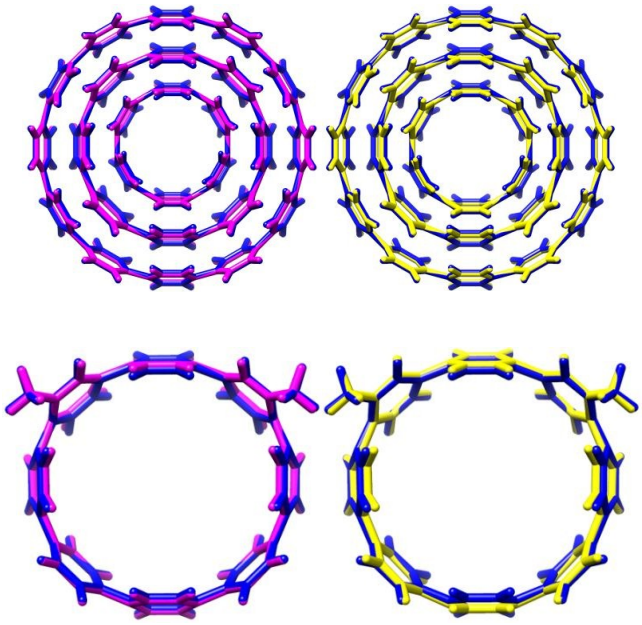

Fig. 2. Comparison between the equilibrium structure of the pristine form (blue) and (left) the reduced form (magenta) or (right) the oxidized form (yellow). (Top) for [n]CPP, from outside to inside [12]CPP, [8]CPP and [6]CPP. The three structures are not shown on the same scale to fit one inside the other. (Bottom) for DMA[8]CPP.

Theoretical methods

Modelling charge transport parameters and rate constants

The charge transport properties are investigated within the non-adiabatic hopping mechanism [44], according to which the charge transfer is localized on a pair of neighbouring molecules (dimer) and the relevant self-exchange process is $M_p + M_{o/r} \leftrightarrow M_{o/r} + M_p$, where M_p is the molecule in its pristine form while $M_{o/r}$ is the molecule in its oxidized/reduced form. The process is mediated by the inter-molecular electronic coupling V_{ij} and associated with a reorganization energy λ.

The molecular materials considered in this work are in crystalline form; therefore, the dimers are identified by evaluating the distances between the centres of mass of the molecules surrounding a central reference molecule in the

View Article Online
DOI: 10.1039/C8CP06727A

crystal. The reliability of the non-adiabatic hopping model depends on the relative magnitude of the electronic couplings (or charge transfer integrals) V_{ij} and the reorganization energy λ, with the former required to be much smaller than the latter [44,45].

Equilibrium structures

Equilibrium structures of pristine and doped (oxidized/reduced) species were obtained from quantum-chemical calculations performed at B3LYP/6-31G* level of theory. The nature of the stationary points obtained by structure optimization was assessed by vibrational frequencies calculations at the optimized structure. Vibrational frequencies were also employed to estimate the vibrational contributions to the intramolecular reorganization energy through the calculations of Huang–Rhys parameters [46-48] (see below).

Note that DMA[8]CPP is a charged species, with high electrostatic interactions in gas-phase causing the computed orbital energies to be largely inaccurate. It has been shown[49] that the large underestimation of the LUMO energy in the gas phase for the family of N-methyl heteroaromatic cations can be corrected once the solvent (acetonitrile) is included using the Conductor-like Polarizable Continuum Model (CPCM)[50,51]. For this reason, gas-phase calculations on DMA[8]CPP were complemented with calculations including solvation (acetonitrile was used as in previous experimental studies[28]). In addition, in the latter case also weak dispersion-like intramolecular noncovalent interactions can be more significant than in [n]CPP, and were consequently included via the D3(BJ) correction term[52,53]. All quantum-chemical calculations were carried out with the Gaussian09 suite of programs.[54]

Intramolecular reorganization energies

The reorganization energy is composed of an intramolecular term λ_i, and an "outer" contribution λ_o due to the interaction with the surrounding molecules in the crystal. The former is computed either with the adiabatic potentials (AP) method, namely via two point determinations from each potential energy surface (pristine and oxidized/reduced state) or via calculations of Huang–Rhys (HR) factors S_m [46-48] in turn obtained from the dimensionless displacement parameters B_m usually employed in the evaluation of the Franck-Condon (FC) vibronic progressions in electronic and photoelectronic spectra. [55,56] The B_m and S_m parameters, assuming the harmonic approximation and neglecting Duschinski rotation, are defined as

$$\boldsymbol{B_m} = \sqrt{\frac{\boldsymbol{\omega_m}}{\hbar}}[\boldsymbol{X_k} - \boldsymbol{X_j}]\boldsymbol{M}^{1/2}\boldsymbol{L_m(k)} \quad (1)$$

$$\boldsymbol{S_m} = \frac{\boldsymbol{1}}{\boldsymbol{2}}\boldsymbol{B_m}^{\boldsymbol{2}} \quad (2)$$

where $X_{k,j}$ is the 3N dimensional vector of the equilibrium Cartesian coordinates of the k,jth state (here the pristine and oxidized/reduced molecular states), $\boldsymbol{M}$ is the 3N×3N diagonal matrix of atomic masses and $L_m(k)$ is the 3N dimensional vector describing the mth normal coordinate of the kth state in terms of mass weighted Cartesian coordinates.

Electronic couplings

The performance of different schemes designed for efficient calculation of intermolecular transfer integrals and site energies for pairs of molecules have been reviewed recently. [48,57-59] In the framework of the dimer approach and one-electron approximation, $V_{ij} = \langle \phi_i \left| \hat{H} \right| \phi_j \rangle$, where $\phi_{i,j}$ are the HOMO or LUMO orbitals of the two monomers forming the dimer (for *p*-type and *n*-type conduction, respectively). As in our previous studies, we adopted a direct approach for the evaluation of electronic interactions V_{ij} [43,60,61] starting from the matrix $\boldsymbol{H}$ containing the non-orthogonalized electronic couplings, which is obtained as

$$\boldsymbol{H} = \boldsymbol{C}_{\boldsymbol{mon}}^{\boldsymbol{T}}\boldsymbol{S}_{\boldsymbol{dim}}\boldsymbol{C}_{\boldsymbol{dim}}\boldsymbol{\varepsilon}_{\boldsymbol{dim}}\boldsymbol{C}_{\boldsymbol{dim}}^{\boldsymbol{T}}\boldsymbol{S}_{\boldsymbol{dim}}\boldsymbol{C}_{\boldsymbol{mon}} \quad (3)$$

where $\boldsymbol{\varepsilon_{dim}}$ is the diagonal matrix of the eigenvalues for the molecular orbitals of the dimer, $\boldsymbol{C_{dim}}$ is the matrix of the eigenvectors of the dimer, $\boldsymbol{S_{dim}}$ is the overlap matrix between atomic orbitals and $\boldsymbol{C_{mon}}$ are the monomer orbitals.

The computed couplings are then transformed in an orthogonalized basis set as

$$\boldsymbol{H}_{\perp} = \boldsymbol{S}^{-\frac{\boldsymbol{1}}{\boldsymbol{2}}}\boldsymbol{H}\boldsymbol{S}^{-\frac{\boldsymbol{1}}{\boldsymbol{2}}} \quad (4)$$

namely performing an orthogonalization on the 2×2 $\boldsymbol{H}$ matrix including the HOMO (or LUMO) orbitals of the two monomers [57,62]. A detailed discussion of the approximations involved in the fragment orbital approach has been reported in previous work [63].

The electronic couplings were always computed at the same level of theory adopted for geometry optimization and for the evaluation of reorganization energy contributions, unless some selected calculations that were carried out with the ωB97XD functional according to recent recommendations. [64]

Charge transfer rate constants

Three models based on Fermi's Golden rule, but with different levels of approximation, were employed to calculate the corresponding charge transfer rate constants k_{CT}: the Marcus theory, the Marcus-Levich–Jortner formulation, and the spectral overlap approach.

Beside the semi-classical Marcus equation for charge transfer, one more suitable formulation of the charge transfer kinetic constant k_{CT}, for the self-exchange process in a molecular dimer, is the Marcus–Levich–Jortner (MLJ) equation [65,66] which includes a quantum correction of the Marcus equation taking into account the quantum nature of the vibrational modes most active in molecular reorganization:

$$\boldsymbol{k_{CT}} = \frac{\boldsymbol{2\pi}}{\hbar}\boldsymbol{V_{ij}^2}\frac{\boldsymbol{1}}{\sqrt{\boldsymbol{4\pi\lambda_{class}k_BT}}}\sum_{\boldsymbol{v}=\boldsymbol{0}}^{\boldsymbol{\infty}}\left[\boldsymbol{exp}(-\boldsymbol{S_{eff}})\frac{\boldsymbol{S_{eff}^v}}{\boldsymbol{v!}} \times \boldsymbol{exp}\left(-\frac{(\Delta($$

(5)

In Eq (5), the contribution from quantum vibrational degrees of freedom is expressed by a single effective vibrational mode of frequency ω_{eff} and associated Huang–Rhys factor S_{eff}. The effective frequency is determined as

View Article Online
DOI: 10.1039/C8CP06727A

$$\omega_{eff} = \sum_m \omega_m \frac{S_m}{\sum_n S_n} \quad (6)$$

and the HR factor S_{eff} is obtained from the relation $\lambda_i = \hbar\omega_{eff} S_{eff}$. Since low-frequency vibrations (below 200 cm^{-1}) can be described classically, their contribution is included in the λ_{class} term, summed with the outer sphere contribution λ_o assumed to be 0.01 eV according to recent determinations [48,67]. ΔG_0 is the free energy associated with the self-exchange process which, in the absence of electric field (which is the assumption here), is set to zero. Details on the parameters used for the calculations can be found in Table S3.

The third expression used in this work is the spectral overlap (SO) formulation derived in the weak coupling regime from the Fermi Golden rule, according to which the rate constant can be recast in terms of the overlap between the vibrational densities of states of the donor and acceptor normalized on an energy scale: [68-70]

$$k_{CT} = \frac{2\pi}{\hbar} V_{ij}^2 J_{ij} \quad (7)$$

where J_{ij} is the Franck–Condon weighted density of states (FCWDS)

$$J_{ij} = \int dE\, D^A(E) D^D(E) \quad (8)$$

which accounts for the vibrations of the molecules and is approximated by the spectral overlap of the densities of states $D^D(E)$ of the donor and $D^A(E)$ of the acceptor. The analogous approach including the vibrational densities involved in the de-excitation of the donor and excitation of the acceptor is frequently used for exciton transfer. Here the spectra correspond to the generation of the reduced/oxidized form of the acceptor and to the reverse process generating the pristine compound for the donor. The spectra were simulated at 300 K by convoluting computed intensities with a Gaussian function having half width at half maximum of 40 meV.

Table 1. B3LYP/6-31G* computed reorganization energies from the adiabatic potential method.

	λ_i^{AP} *p*-type	λ_i^{AP} *n*-type
[6]CPP	0.362	0.381
[8]CPP	0.259	0.299
[12]CPP	0.171	0.175
DMA[8]CPP	0.330 (0.312) [a]	0.236 (0.298) [a]

[a] calculations carried out in acetonitrile, with the CPCM model and intra-molecular dispersion interactions with the D3(BJ) correction term.

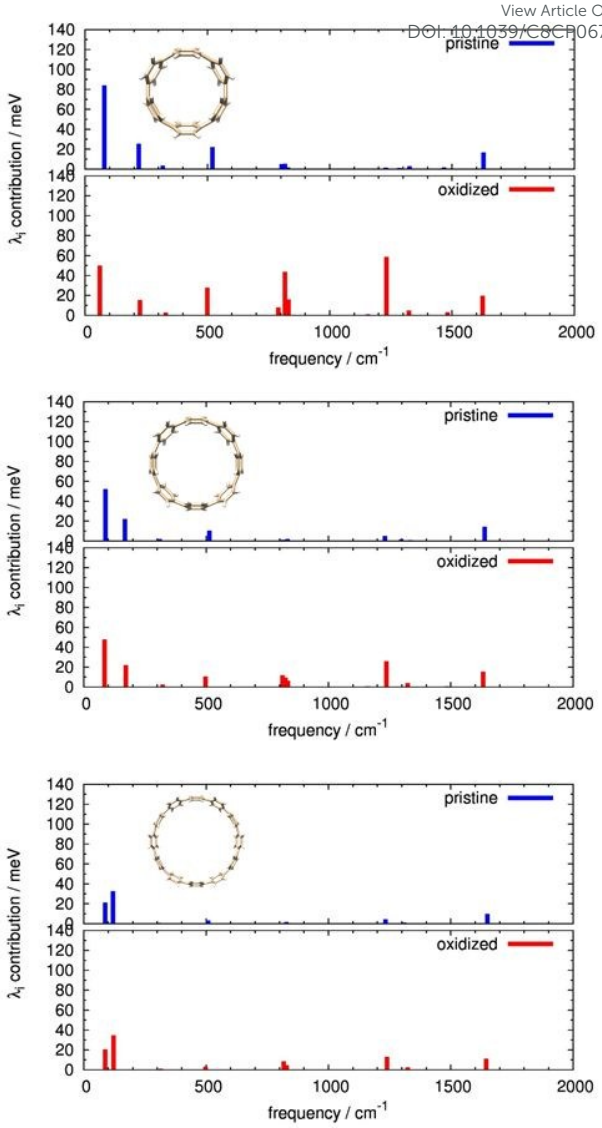

Fig. 3. The vibrational frequency contributions (from HR factors) to the computed intramolecular reorganization energies (for p-type charge transport) of [6]CPP (top), [8]CPP (middle) and [12]CPP (bottom). Each graph shows the contribution from pristine species on the top and from the oxidized species in the bottom part. From B3LYP/6-31G* calculations.

Results and discussion

Geometry changes upon charge transport

The equilibrium structures were computed for the pristine, oxidized and reduced forms of each nanohoop. The most symmetric structures, belonging to the $D_{(n/2)d}$ point group for [n]CPPs and C_s point group for DMA[8]CPP were always considered.

View Article Online
DOI: 10.1039/C8CP06727A

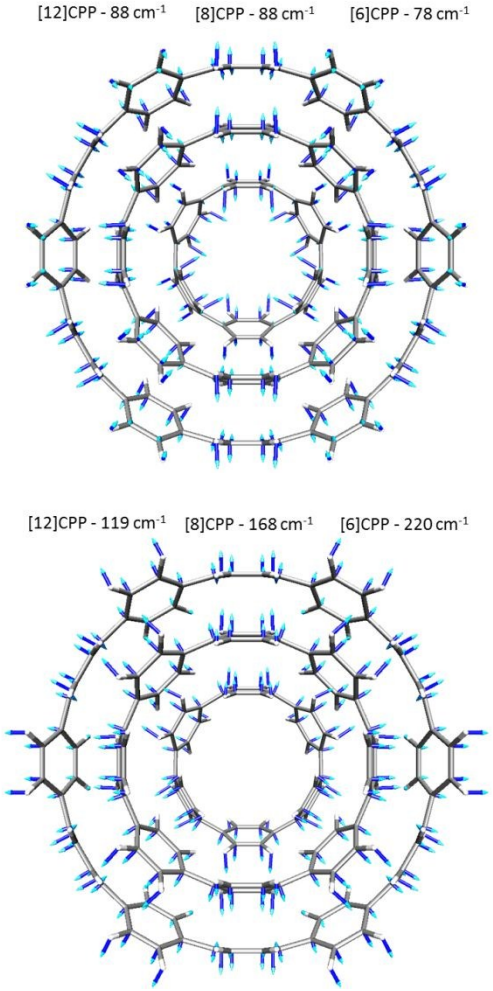

Fig. 4 Graphical representation of the low frequency vibrational normal modes (B3LYP/6-31G*, pristine molecule) contributing to the reorganization energy of the [n]CPP series. The mode in the bottom part is the ring breathing mode whose frequency is diagnostic of the size of the nanohoop. From outside to inside [12]CPP, [8]CPP and [6]CPP. The three structures are not in the same scale: They were rescaled to fit one inside the other.

The superposition of the optimized geometries of the pristine (blue) and reduced (magenta) forms are shown in the top part of Fig. 2 for the three [n]CPP systems investigated. The structure of the reduced form of each nanoring is less twisted than the pristine molecule, as a result of the increase of quinoidal character. [17, 36] Similar considerations hold for the oxidized structures depicted in yellow on the right side of Fig. 2. Even in this case the structures show a decrease of twisting between adjacent rings characterizing the oxidized species, in agreement with the observed structures of cationic and anionic CPPs. [12-16] A graphical comparison between equilibrium structures of reduced and oxidized species can be seen in Fig. S2, showing a similar twisting for the two species, with the oxidized form (yellow) displaying a systematically smaller diameter than the reduced form (magenta). Similar geometrical changes occur for DMA[8]CPP except that the reduced symmetry (C_s) of the D-A derivative is reflected in a slightly elliptic shape of the nanoring, less marked for the oxidized and reduced forms which, similarly to [n]CPPs, are characterized by a reduction of the twisting between adjacent rings, in account of the more rigid quinoidal structure (see the bottom part of Fig. 2, same colour code as for [n]CPPs). The effect of including intermolecular dispersion corrections can be seen in Fig. S3 for the geometry of pristine DMA[8]CPP, showing a less elliptical shape of the nanoring (cyan colour code) when dispersion interactions (and solvent via CPCM) are included. Because of the reduced symmetry of DMA[8]CPP associated with the D-A character which implies molecular orbitals localized on two different molecular moieties (see the frontier molecular orbitals in Fig. S4), the structural changes upon reduction/oxidation are localized on the N-doped moiety / phenylene moiety respectively. This can be appreciated by inspecting Fig. 2 (bottom), Fig. S5 and S6 in the ESI, showing the large geometry difference between oxidized and reduced forms of DMA[8]CPP compared to the case of [n]CPPs.

Reorganization energies: the role of torsional and RBM modes

The above discussed geometry changes are reflected in the reorganization energies associated with charge transport. For all the systems tackled we determined the reorganization energies for the most symmetric structures too. These do not fully correspond to the structures found in the crystals, mostly due to librational disorder, but we have verified that less symmetric conformers display modest differences in reorganization energies. Therefore, those determined for the most symmetric structures can be considered representative also for the conformers in the solid phase. In addition, the use of the highly symmetric structures allows to determine with accuracy (due to the reduced number of totally-symmetric (TS) vibrations contributing to B_m parameters) the contributions of vibrational normal modes to the reorganization energies, via calculation of HR factors. Using less symmetric conformers leads, indeed, to a wide distribution of small S_m contributions that are far less clear-cut, as it will be shown for DMA[8]CPP.

The reorganization energies computed according to the AP method for the $D_{(n/2)d}$ geometries of [n]CPPs are collected in Table 1 and S3. The computed values agree with those obtained in a previous investigation [36] and decrease with the increase of the dimension (i.e. number of conjugated units) of the nanoring as it was expected. In the same Tables we also include the AP results for DMA[8]CPP. Note that the two N-methyl substituents may lie on the same side of the nanoring plane (cis- conformer), in which case a C_s symmetry structure can be determined, or they can lie on opposite sides, leading to a trans- conformer which is less symmetric, less stable by ca. 2 kcal/mol (see Table S1) but is the structure observed in the crystalline phase. The reorganization energies of the trans- and cis- conformers differ by only 6 meV for *p*-type charge transport and by 20 meV for *n*-type charge transport. Owing to these small differences, we restrict the attention on the cis-conformer and note that it displays a larger reorganization energy for *p*-type transport compared to the parent [8]CPP (330 meV versus 259 meV, respectively) while the opposite occurs for *n*-type charge transport (236 meV versus 299 meV, respectively). Notably, the effect of including dispersion

interactions (and solvent effects) leads to an equalization of the reorganization energies for *p*-type and *n*-type transport, both resulting close to ca. 300 meV (see Table 1). Thus, from the point of view of reorganization energy we can conclude that there is no net prevalence between *p*-type and *n*-type transport for DMA[8]CPP, a sign already of some ambipolar character.

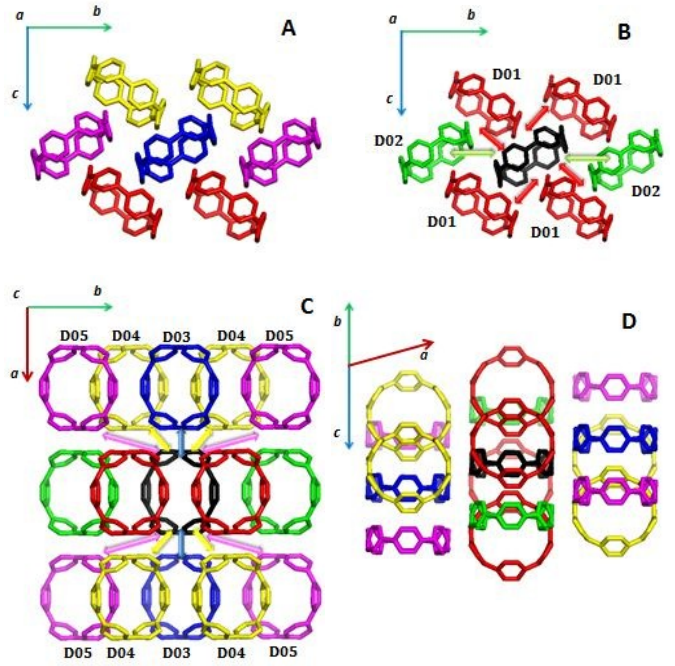

Fig. 5. Charge transport paths for the crystal of [6]CPP. (A) view of the near neighbours in the *bc* plane; (B) selected near neighbours in the *bc* plane and the available charge paths D01, D02 indicated by arrows. (C) view of the near neighbours in the *ab* plane: The coloured arrows indicate the available charge paths D03, D04 and D05 from the black central ring; (D) view of the neighbours showing the misalignment between nanohoops along path D03 and D05. Hydrogen atoms omitted for clarity.

To acquire further information on the vibrational modes that assist charge transport by contributing to reorganization energies, we computed the HR factors for the three highly symmetric CPP nanohoops and collect a graphical representation of the vibrational contributions in Fig. 3 for *p*-type charge transport, and in Fig. S7 for *n*-type charge transport. While for most organic semiconductors the largest contributions arise for modes generally above 1000 cm^{-1}, CPP nanorings reveal the role of two low frequency vibrations remarkably contributing to reorganization energies: a) the ring torsional modes and b) the already mentioned RBMs (see Fig. 4 for a pictorial representation of the low frequency TS modes). The latter modes are diagnostic of the size of the nanoring and were previously experimentally identified in Raman spectra investigations[17]. We note that the contribution of the RBM, whose frequency decreases from [6]CPP to [12]CPP, becomes more important compared to the torsional mode. The geometry changes associated with charge hopping, described in the previous section (reduced twisting for both oxidized and reduced species along with compression of the ring for the oxidized forms), justify the significant contributions of these two modes that becomes close to 50% of the reorganization energy for the largest nanoring.

We note that the activity of low frequency modes will also be reflected in the magnitude of computed rate constants since these modes can be considered to a good approximation classical modes, especially for the larger nanohoops.

Beside low frequency modes, other active modes are found at ca. 500 cm^{-1}, 1230 cm^{-1} and 1630 cm^{-1} (see Fig. S7 and S8). All these are related to benzene vibrational normal modes and are less diagnostic of the size of the ring, with frequencies undergoing very small changes with the dimension of the nanohoop.

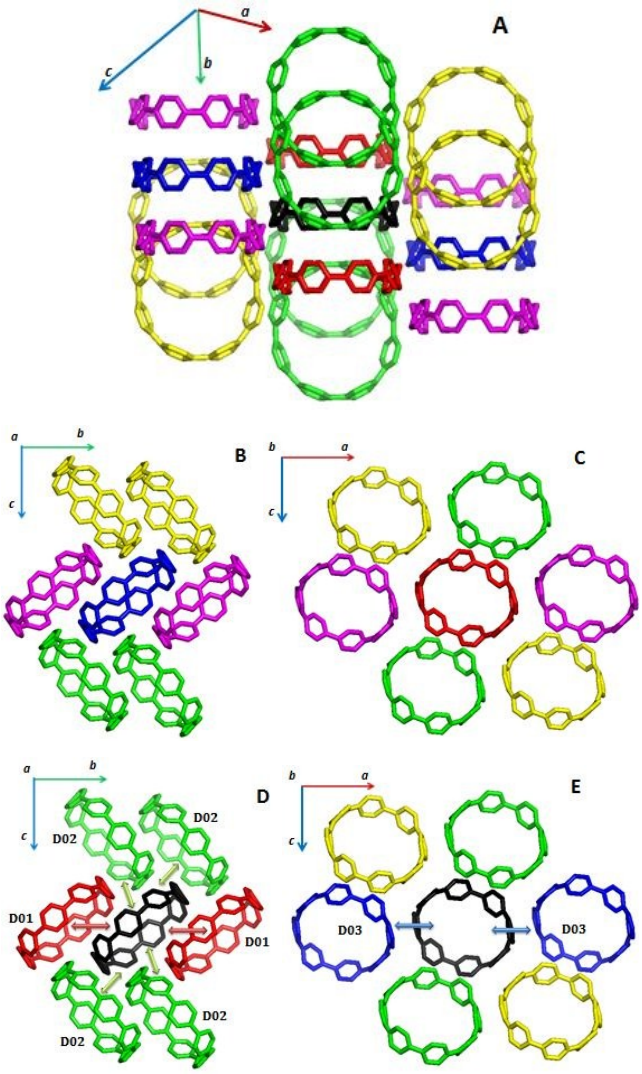

Fig. 6. Charge transport paths for the crystal of [8]CPP. (A) view of all the neighbours of the central black molecule considered in calculations; (B) view of the near neighbours in the *bc* plane; (C) view of the near neighbours in the *ac* plane; (D) same as B but only the nanohoops belonging to one layer are shown: The arrows show the available charge paths D01 and D02 from the black central ring; (E) same as C but with fewer molecules to show the available charge path D03 from the black central ring; the misalignment between nanohoops along path D03 can be appreciated in panel A. More details concerning paths D04 and D05 in the ESI. Hydrogen atoms omitted for clarity.

Moving to DMA[8]CPP, owing to the reduced symmetry and increased number of TS modes, the computed vibrational

contributions are less clear to identify because small contributions arise from a large number of modes with similar frequencies. Nevertheless, using as a guide the parent [8]CPP (see Fig. S9, S10) a close relation with the more symmetric [n]CPPs can be found: for instance a remarkable contribution comes from low frequency modes related to the RBM mode and most of the other contributions are computed for frequencies in the 1200-1600 cm^{-1} range. We note in particular that the pattern of HR active vibrations follows slightly more closely that of [8]CPP when calculations on DMA[8]CPP are carried out including dispersion interactions (bottom panel in both figures).

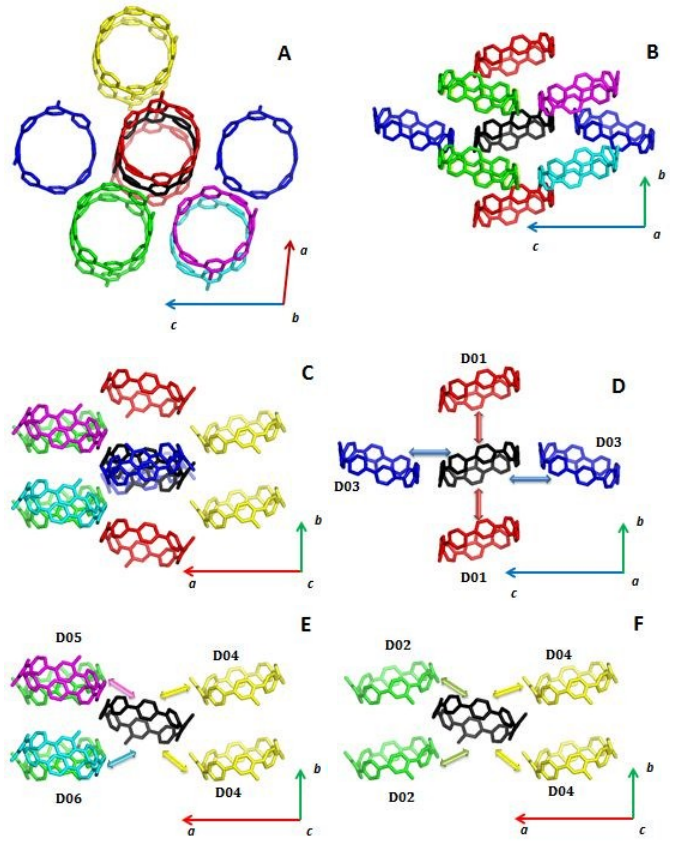

Fig. 7. Charge transport paths for the crystal of DMA[8]CPP. (A) View, in the *ac* plane, of all the neighbours of the central black molecule considered in calculations; (B) view of the near neighbours in the *bc* plane; (C) view of the near neighbours in the *ab* plane; (D) same as (B) but with fewer molecules to show (coloured arrows and labels) the available charge paths D01 and D03 from the black central ring; (E) and (F) same as (C) but with fewer molecules to show the available charge path D02, D04, D05, D06 from the black central ring. Hydrogen atoms omitted for clarity.

Table 2. Electronic couplings V_{ij} (B3LYP/6-31G* level of theory unless specified) computed for the different charge hopping paths in the crystals of [n]CPP (n=6,8,12) and DMA[8]CPP.

Dimer	Center of mass distance (Å)	V_{ij}^{HOMO} (meV)	V_{ij}^{LUMO} (meV)
		[6]CPP	
D01	7.6388	10 (10)[a]	10 (14)[a]
D02	10.3120	5 (5)[a]	24 (27)[a]
D03	11.1772	29 (33)[a]	27 (31)[a]
D04	12.1597	8 (10)[a]	11 (12)[a]
D05a	15.2075	0 (0)[a]	0 (0)[a]
D05b	15.2075	0 (0)[a]	0 (0)[a]
		[8]CPP	
D01	8.0103	1 (1)[a]	3 (3)[a]
D02	10.8835	8 (9)[a]	11 (12)[a]
D03	12.9325	16 (17)[a]	10 (11)[a]
D04	13.5944	6 (6)[a]	16 (18)[a]
D05a	15.2123	5 (5)[a]	7 (8)[a]
D05b	15.2123	0 (0)[a]	0 (0)[a]
		[12]CPP	
D01	8.1878	0 (0)[a]	4 (4)[a]
D02	12.5231	0 (0)[a]	2 (2)[a]
D03	18.5827	3 (3)[a]	21 (21)[a]
D04	19.4871	1 (1)[a]	12 (13)[a]
D05a	20.3066	6 (6)[a]	10 (12)[a]
D05b	20.3066	0 (0)[a]	0 (0)[a]
		DMA[8]CPP	
D01	10.3840	0 (0)[b]	0 (0)[b]
D02	13.8313	9 (5)[b]	3 (1)[b]
D03	13.9330	0 (2)[b]	0 (1)[b]
D04	14.5269	0 (0)[b]	3 (3)[b]
D05	14.8949	113 (97)[b]	2 (2)[b]
D06	14.9185	0 (0)[b]	0 (0)[b]

[a] Calculations carried with the ωB97XD functional.

[b] Calculations carried out in acetonitrile described with the CPCM model and intra-molecular dispersion interactions with the D3(BJ) correction term.

Electronic couplings and charge transport rate constants: from CPPs to D-A-CPPs

A detailed investigation on dimers and electronic couplings can clarify which molecular orientations are most favourable to maximize charge transport.

[6]CPP, [8]CPP and [12]CPP. Recently a new polymorph of [6]CPP from solvent-free deposition was obtained displaying a solid state packing switching from a tubular-like to a herringbone arrangement. [16] We thus analysed the crystal and determined the nearest neighbours of a central molecule depicted in black in Fig. 5 and S11. The centre of mass distances for the molecular dimers identified with different colour codes and labels in Fig. 5, are collected in Table S4. The computed electronic couplings are collected in Table 2. The couplings computed using the ωB97XD functional are very similar to those computed with B3LYP and therefore in the following we will restrict the discussion to the latter set of values. Molecules are arranged in a herringbone fashion

forming layers, however the largest couplings for both *n*-type and *p*-type transport are computed for the hopping between molecules belonging to two different layers (dimer labelled D03 in Fig. 5). Note that this is in contrast with the majority of known molecular semiconductors where the layer in which molecules are arranged identifies the largest electronic couplings. Hopping between molecules whose centres of mass are closer, such as for dimers D01 and D02, display smaller couplings. In one case (D02) we note that the coupling is larger for *n*-type transport compared to *p*-type and we suspect that molecular fluctuations induced by thermal effects may be of some relevance to increase the *p*-type coupling as previously noted for some PBI derivatives[38]. Finally other inter-layer couplings such as D04 are quite small and D05 are negligible although they become more and more relevant for the higher members in the series of CPPs.

The crystal structure of [8]CPP [21] shows an arrangement of nanorings similar to the new polymorph of [6]CPP, organized in layers in which molecules are packed herringbone. A visual representation of the nearest neighbours of a given nanoring is depicted in Fig. 6 and S12. Similarly to [6]CPP, the largest couplings are computed for the D03 dimer (hopping between layers) although the magnitude of the couplings has decreased compared to the smaller nanohoop. The inter-layer hopping via D04 path shows a comparably larger coupling for *n*-type transport, probably for a similar reason as for [6]CPP: the optimal packing induced by intermolecular forces in organic crystals corresponds, in some cases, to minimization of the molecular orbital superposition and of the corresponding electronic couplings. The inter-layer path D05a is the same as for [6]CPP (see Fig. S11 and S12) with two pairs of molecules in a slipped-lateral arrangement but for [8]CPP the molecules are better aligned and result in a larger coupling. This coupling increases further (see Table 2) moving to the crystal structure of [12]CPP [20] whose pattern of possible paths for charge transport are shown in Fig. S13. The alignment between molecules forming the dimer D05a is very efficient to maximize the interaction in this case. The largest couplings are however computed for the inter-layer path D03 as for the smaller CPPs.

In summary, our calculations suggest that electronic couplings for tubular arrangements are generally negligible, as found also before[36], and those for herringbone arrangements are not optimal while, owing to the possible larger orbital overlap, those for slipped lateral arrangements are the most favourable. Therefore, contrary to most planar organic semiconductors where the layer in which molecules are herring-bone arranged identifies the high-mobility plane, nanohoops disclose an inter-layer charge transport (due to the above discussed slipped-lateral arrangements) more efficient than the intra-layer counterpart. Finally we note that these computed coupling are substantially smaller than those computed previously [36] but are in line with the expected values on the basis of the overlap between electron clouds. Indeed the not optimal reciprocal orientation of two molecules is one factor limiting the couplings in the crystal. Another factor is that two molecules in the [n]CPP crystal are never aligned on the same plane. We ascribe the differences with previous investigations to the overestimation of the approach employed there, an upper limit indeed according to recent investigations showing a pronounced dependence of electronic couplings on Hartree-Fock exchange. [71]

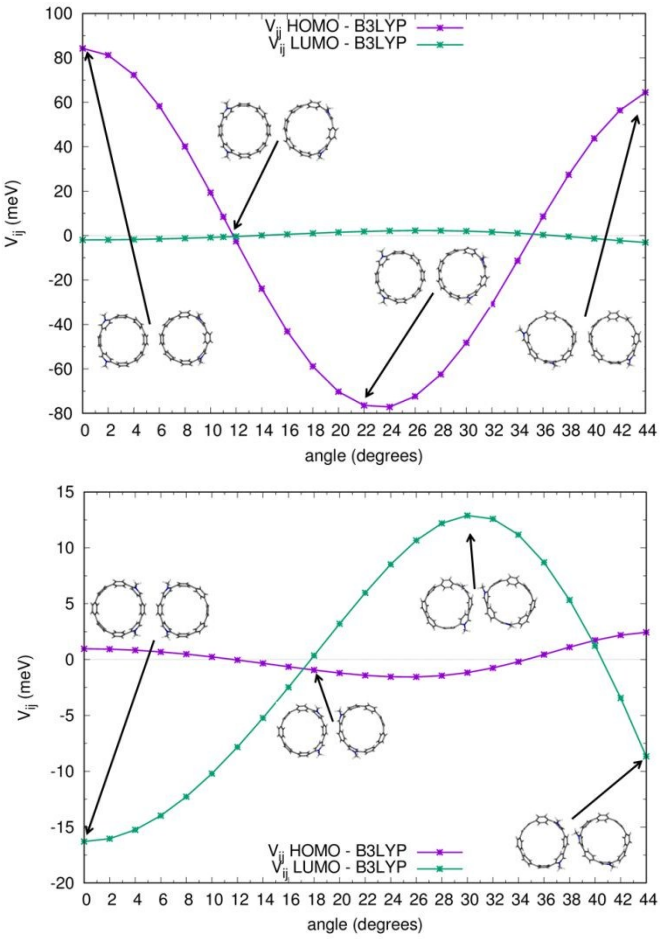

Fig. 8. Electronic couplings computed for a model dimer of DMA[8]CPP upon rotation of one molecule with respect to the other, showing the modulation of couplings. (top) Configuration favouring p-type interaction, (bottom) configuration favouring n-type interaction.

DMA[8]CPP. The crystal structure of DMA[8]CPP includes solvent molecules and counter-ions [28] that were removed to analyse the available paths for charge transport collected in Fig. 7. Each nanohoop in the crystal structure has one face centred D-A interaction between its own pyridinium ring and a neighbour's electron-rich phenylene ring. The layers that make up the third dimension of the crystal structure form tubular-like channels. Considering the couplings discussed above for [n]CPPs, one would expect the largest values for molecules adopting the slipped lateral arrangement. More specifically, dimers D03 and D05 display the most favourable face to face arrangement. However in the D03 dimer the donor ring of one molecule is faced with the acceptor side of the other molecule. Because the LUMO orbital is localized on the acceptor moiety and the HOMO orbital is localized on the donor moiety, the electronic coupling for either *n*-type or *p*-type is expected to be modest for this dimer, as confirmed by the calculations (see

Table 2). Dimer D05 shows, in contrast, a favourable orientation for maximizing the *p*-type electronic interaction (see panels A and E in Fig.7) which is confirmed by the large computed coupling amounting to 113 meV and overtaking all those results computed for [n]CPPs.

Table 3. Charge transfer rate constants k_{CT} (ps^{-1}) computed for the most efficient charge hopping paths available in the crystals of [8]CPP and DMA[8]CPP.

[8]CPP *p*-type

	k_{CT}/ps^{-1}		
Dimer	*Marcus*	*MLJ*	*SO*
D02	0.15	0.22	0.36
D03	0.55	0.84	1.36
D04	0.07	0.11	0.17
D05a	0.05	0.07	0.11

[8]CPP *n*-type

	k_{CT}/ps^{-1}		
Dimer	*Marcus*	*MLJ*	*SO*
D02	0.16	0.34	0.52
D03	0.13	0.29	0.44
D04	0.32	0.70	1.07
D05a	0.06	0.14	0.20

DMA[8]CPP *p*-type

	k_{CT}/ps^{-1}		
Dimer	*Marcus*	*MLJ*	*SO*
D02	0.08	0.16	0.20
D05	13.1	25.5	31.3

DMA[8]CPP *n*-type

	k_{CT}/ps^{-1}		
Dimer	*Marcus*	*MLJ*	*SO*
D02	0.02	0.03	0.05
D04	0.02	0.03	0.06
D05	0.01	0.01	0.03

Model dimers of DMA[8]CPP. The significant increase of the coupling determined for *p*-type conduction in the crystal of DMA[8]CPP suggests that appropriate orientation of the D-A nanorings in the solid state tunes the magnitude of the electronic interaction, due to orbital localization. To further explore this concept and support the evidence of such increased coupling, we have carried out calculations on a model dimer formed by two DMA[8]CPP molecules. We selected two arrangements: a) the donor moieties of the two molecules forming the dimer are faced to maximize the overlap between HOMOs or b) the acceptor moieties are faced to maximize the overlap between LUMOs. The graphs depicting the dependence of the couplings with respect to the distance between the centres of mass (Fig. S14 and S15), show that couplings between HOMOs can reach larger values than couplings between LUMOs, suggesting that these D-A nanohoops are better suited for *p*-type charge transport. In Fig. 8 and S16 we consider the rotation of one nanohoop with respect to the other, starting from the same configurations as above with a distance between faced phenyl rings in the model dimers of ca. 4.1 Å. Changing the reciprocal orientation modulates the coupling in an oscillatory way, either for *n*-type and *p*-type transport. The modulation follows the oscillations in orbital overlap, from a (large absolute) value when one ring in one nanohoop is facing a ring in the other molecule to a value close to zero when facing the CC bond connecting two rings.

Computed rate constants. The rate constants for the most efficient charge transport paths of [8]CPP and DMA[8]CPP, evaluated with Marcus, MLJ and SO formulations, are collected in Table 3 (for the complete set of paths see Tables S6, S7). The differences above discussed in intra-molecular and inter-molecular charge transport parameters are reflected in remarkable differences between the largest computed rate constant of [8]CPP and DMA[8]CPP. The latter shows a potentially more efficient *p*-type charge transport (23 times larger rate constant) while [8]CPP displays more efficient *n*-type charge transport (18 times larger rate constant). We note however that owing to charge localization, DMA[8]CPP can become more efficient also for *n*-type charge transport if a suitable solid state packing can be realized. Comparing the results of the three approaches employed to evaluate rate constants, we note that the SO approach predicts the largest values, MLJ intermediate while Marcus theory predicts the smallest values. From the viewpoint of quantum chemical calculations, the Marcus theory is much easier, since, instead of explicitly calculating the spectral overlap from the Franck–Condon factors, it is sufficient to calculate the reorganization energy λ. However it does not account for quantum effects which may be relevant given the presence of high frequency vibrations assisting the charge transfer. Our results are in good agreement with recent investigations on exciton diffusion in which Marcus theory was found to predict smaller values than the SO approach, in turn providing results in agreement with experiment. [70] In another study the Marcus and MLJ formulations were found to overestimate computed charge transport rate constants of oligoacenes [69] in contrast with the SO approach. These investigations suggest that the SO approach, which is also the most expensive computationally, provides more reliable values in comparison with the other two. The present study is in line with the results of ref. [70] owing to the fact that, for the nanohoops investigated the non-adiabatic hopping model is a good approximation, being the relation $\boldsymbol{V_{ij} \ll \lambda}$ always verified.

Conclusions

The intra-molecular and inter-molecular charge transport parameters have been computed for [n]CPPs (n=6,8,12) and a D-A derivative DMA[8]CPP recently synthesized and crystallized. The geometry changes upon reduction / oxidation of [n]CPPs and DMA[8]CPP have been determined both with the AP and the HR factors approaches. For [n]CPPs the oxidized/reduced forms have similar structures, characterized by a reduced twisting of phenyl rings, uniformly distributed over the nanoring, with an overall shrinking of the oxidized ring compared to reduced form. In contrast, for DMA[8]CPP geometry changes are strongly localized on the donor or acceptor moieties for the oxidized / reduced forms respectively. Interestingly, although the symmetry is largely reduced in DMA[8]CPP, a similar contribution of

intramolecular vibrations to charge transport was determined via calculations of HR factors.

A very peculiar character of the nanorings compared to most conjugated organic semiconductors is the substantial contribution of low frequency modes: the twisting of adjacent phenyl rings and the RBM previously detected in Raman measurements.

The pathways available for charge transport have been identified employing available crystal structures and it has been shown that contrary to most planar organic semiconductors where the layer in which molecules are herring-bone arranged identifies the high-mobility plane, nanohoops disclose inter-layer charge transport more efficient than the intra-layer counterpart. The detailed investigation on dimers and electron couplings clarifies which molecular orientations are most favourable to maximize charge transport. When moving from CPPs to D-A derivatives, the role of orbital localization on the donor or acceptor moieties introduces an additional orientation factor that clearly emerges from the analysis of dimers and suggests design rules. Indeed, the study shows that *p*-type charge transfer is more efficient for the crystal of DMA[8]CPP than [8]CPP, but calculations on model dimers suggested that also *n*-type charge transport can become more efficient if a suitable solid state packing can be realized. The optimization of the solid state phases of D-A nanohoops may result in tuning either *n*-type or *p*-type charge transport, thus disclosing useful structure-property relationships to be further exploited.

Conflicts of interest

There are no conflicts to declare.

Acknowledgements

FN and SC acknowledge financial support from the University of Bologna. AJPJ and JCSG acknowledge the "Ministerio de Economía y Competitividad" of Spain and the "European Regional Development Fund" through the project CTQ2014-55073-P.

Notes and references

1 H. Omachi, Y. Segawa, K. Itami, "Synthesis of Cycloparaphenylenes and Related Carbon Nanorings: A Step toward the Controlled Synthesis of Carbon Nanotubes", *Acc. Chem. Res*., 2012, **45**, 1378–1389.

2 M. R. Golder, R. Jasti, "Syntheses of the Smallest Carbon Nanohoops and the Emergence of Unique Physical Phenomena", *Acc. Chem. Res*., 2015, **48**, 557–566.

3 X. Lu, J. Wu, "After 60 Years of Efforts: The Chemical Synthesis of a Carbon Nanobelt", *Chem*, 2017, **2**, 610–620.

4 K. Okada, A. Yagi, Y. Segawa and K. Itami, "Synthesis and properties of [8]-, [10]-, [12]-, and [16]- cyclo-1,4-naphthylenes", *Chem. Sci*., 2017, **8**, 661.

5 U. Bunz, S. Menning, N. Martín, "Para-Connected Cyclophenylenes and Hemispherical Polyarenes: Building Blocks for Single- Walled Carbon Nanotubes", *Angew. Chem. Int. Ed.*, 2012, **51**, 7094−7101.

6 G. Povie, Y. Segawa, T. Nishihara, Y. Miyauchi, K. Itami, "Synthesis of a carbon nanobelt", *Science*, 2017, **356**, 172–175.

7 G. Povie, Y. Segawa, T. Nishihara, Y. Miyauchi, K. Itami, "Synthesis and Size-Dependent Properties of [12], [16], and [24]Carbon Nanobelts", *J. Am. Chem. Soc.,* 2018, **140**, 10054-10059.

8 H. A. Wegner, "On the Way to Carbon Nanotubes: The First Synthesis of an Aromatic Nanobelt", *Angew. Chem. Int. Ed.*, 2017, **56**, 10995 – 10996.

9 T. Iwamoto, Y. Watanabe, Y. Sakamoto, T. Suzuki, S. Yamago, "Selective and Random Syntheses of [n]Cycloparaphenylenes (n=8−13) and Size Dependence of Their Electronic Properties", *J. Am. Chem. Soc.*, 2011, **133**, 8354−8361.

10 Y. Segawa, A. Fukazawa, S. Matsuura, H. Omachi, S. Yamaguchi, S. Irle, K. Itami, "Combined experimental and theoretical studies on the photophysical properties of cycloparaphenylenes", *Org. Biomol. Chem*., 2012, **10**, 5979–5984.

11 L. Adamska, I. Nayyar, H. Chen, A. K. Swan, N. Oldani, S. Fernandez-Alberti, M. R. Golder, R. Jasti, S. K. Doorn, S. Tretiak, "Self-Trapping of Excitons, Violation of Condon Approximation, and Efficient Fluorescence in Conjugated Cycloparaphenylenes", *Nano Lett*., 2014, **14**, 6539–6546.

12 E. Kayahara, T. Kouyama, T. Kato, H. Takaya, N. Yasuda and S. Yamago, "Isolation and Characterization of the Cycloparaphenylene Radical Cation and Dication", *Angew. Chem. Int. Ed.*, 2013, **52**, 13722.

13 M. R. Golder, B. M. Wong, R. Jasti, "Photophysical and theoretical investigations of the [8] cycloparaphenylene radical cation and its charge resonance dimer", *Chem. Sci.*, 2013, **4**, 4285.

14 N. Toriumi, A. Muranaka, E. Kayahara, S. Yamago, M. Uchiyama, "In-Plane Aromaticity in Cycloparaphenylene Dications: A Magnetic Circular Dichroism and Theoretical Study", *J. Am. Chem. Soc*., 2015, **137**, 82–85.

15 A. V. Zabula, A. S. Filatov, J. Xia, R. Jasti, M. A. Petrukhina, "Tightening of the Nanobelt upon Multielectron Reduction", *Angew. Chem. Int. Ed.*, 2013, **52**, 5033 –5036.

16 S. N. Spisak, Z. Wei, E. Darzi, R. Jasti, M. A. Petrukhina, "Highly strained [6]cycloparaphenylene: crystallization of an unsolvated polymorph and the first mono- and dianions", *Chem. Comm.*, 2018, **54**, 7818-7821.

17 M. Peña-Alvarez, P. M. Burrezo, M. Kertesz, T. Iwamoto, S. Yamago, J. Xia, R. Jasti, L. J. T. Navarrete, M. Taravillo, V. G. Baonza, J. Casado, "Properties of Sizeable [n]Cycloparaphenylenes as Molecular Models of Single-Wall Carbon Nanotubes Elucidated by Raman Spectroscopy: Structural and Electron-Transfer Responses under Mechanical Stress", *Angew. Chem. Int. Ed.*, 2014, **53**, 7033–7037.

18 M. Peña-Alvarez, M. C. Ruiz Delgado, M. Taravillo, V. G. Baonza, J. T. Lopez Navarrete, P. Evans, R. Jasti, S. Yamago, M. Kertesz, J. Casado, "The Raman Fingerprint of Cyclic Conjugation: The case of the Stabilization of Cations and Dications in Cycloparaphenylenes", *Chem. Sci*., 2016, **7**, 3494–3499.

19 M. Peña-Alvarez, L. Qiu, L. M. Taravillo, V. G. Baonza, M. C. Ruiz Delgado, S. Yamago, R. Jasti, J. T. Lopez Navarrete, J. Casado, M. Kertesz, "From linear to cyclic oligoparaphenylenes: electronic and molecular changes traced in the vibrational Raman spectra and reformulation of the bond length alternation pattern", *Phys. Chem. Chem. Phys*., 2016, **18**, 11683–11692.

20 Y. Segawa, S. Miyamoto, H. Omachi, S. Matsuura, P. Senel, T. Sasamori, N. Tokitoh, K. Itami, "Concise Synthesis and Crystal Structure of [12]Cycloparaphenylene", *Angew. Chem. Int. Ed*., 2011, **50**, 3244 –3248.

21 J. Xia, J. W. Bacon, R. Jasti, "Gram-scale synthesis and crystal structures of [8]- and [10]CPP, and the solid-state structure of C60@[10]CPP", *Chem. Sci.*, 2012, **3**, 3018.

22 M. R. Wasielewski, "Photoinduced electron transfer in supramolecular systems for artificial photosynthesis", *Chem. Rev*., 1992, **92**, 435–461.

23 Y. Wu, W. Zhu, "Organic sensitizers from D-π-A to DA-π-A: effect of the internal electron-withdrawing units on molecular absorption, energy levels and photovoltaic performances", *Chem. Soc. Rev*., 2013, **42**, 2039 – 2058.

24 M. Ball, B. Fowler, P. Li, L. A. Joyce, F. Li, T. Liu, D. Paley, Y. Zhong, H. Li, S. Xiao, F. Ng, M. L. Steigerwald, C. Nuckolls, "Chiral Conjugated Corrals", *J. Am. Chem. Soc*., 2015, **137**, 9982−9987.

25 M. Ball, Y. Zhong, B. Fowler, B. Zhang, P. Li, G. Etkin, D. W. Paley, J. Decatur, A. K. Dalsania, H. Li, S. Xiao, F. Ng, M. L. Steigerwald, C. Nuckolls, "Macrocyclization in the Design of Organic n‐Type Electronic Materials", *J. Am. Chem. Soc.*, 2016, **138**, 12861−12867.

26 S. Nishigaki, M. Fukui, H. Sugiyama, H. Uekusa, S. Kawauchi, Y. Shibata, K. Tanaka, "Synthesis, Structures, and Photophysical Properties of Alternating Donor–Acceptor Cycloparaphenylenes", *Chem. Eur. J.*, 2017, **23**, 7227 – 7231.

27 T. Kuwabara, J. Orii, Y. Segawa, K. Itami, "Curved Oligophenylenes as Donors in Shape-Persistent Donor–Acceptor Macrocycles with Solvato-fluorochromic Properties", *Angew. Chem. Int. Ed.*, 2015, **54**, 9646 –9649.

28 J. M. Van Raden, E. R. Darzi, L. N. Zakharov, R. Jasti, "Synthesis and characterization of a highly strained donor-acceptor nanohoop", *Org. Biomol. Chem*., 2016, **14**, 5721.

29 E. R. Darzi, E. S. Hirst, C. D. Weber, L. N. Zakharov, M. C. Lonergan, R. Jasti, "Synthesis, Properties and Design Principles of Donor-Acceptor Nanohoops.", *ACS Cent. Sci*., 2015, **1**, 335.

30 L. Tan, Y. Guo, Y. Yang, G. Zhang, D. Zhang, G. Yu, W. Xu, Y. Liu, "New tetrathiafulvalene fused-naphthalene diimides for solution-processible and air-stable *p*-type and ambipolar organic semiconductors", *Chem. Sci*., 2012, **3**, 2530-2541.

31 E. San-Fabián, A. Pérez-Guardiola, M. Moral, A. J. Pérez-Jiménez, J. C. Sancho-García, "Theoretical Study of Strained Carbon-based Nanobelts: Structural, Energetic, Electronic, and Magnetic Properties of [n]Cyclacenes", in *Adv. Magn. Opt. Mater.,* 2016, Wiley Online library, Chapter 6, pp 165–183.

32 M. Reche-Tamayo, M. Moral, A. J. Pérez-Jiménez, J. C. Sancho-García, "Theoretical Determination of Interaction and Cohesive Energies of Weakly Bound Cycloparaphenylene Molecules", *J. Phys. Chem. C*, 2016, **120**, 22627–22634.

33 J. V. Climent-Medina, A. J. Pérez-Jiménez, M. Moral, E. San-Fabián, J. C. Sancho-García, "Intra- and Intermolecular Dispersion Interactions in [n]Cycloparaphenylenes: Do They Influence Their Structural and Electronic Properties?", *Chem. Phys. Chem.,* 2015, **16**, 1520-1528.

34 A. Pérez-Guardiola, M. E. Sandoval-Salinas, D. Casanova, E. San-Fabián, A. J. Pérez-Jiménez, J. C. Sancho-García, "The role of topology in organic molecules: origin and comparison of the radical character in linear and cyclic oligoacenes and related oligomers", *Phys. Chem. Chem. Phys.*, 2018, **20**, 7112-7124.

35 C. Graham, M. Moral, L. Muccioli, Y. Olivier, A. J. Pérez-Jiménez, J. C. Sancho-García, "N-doped cycloparaphenylenes: Tuning electronic properties for applications in thermally activated delayed fluorescence", *Int. J. Quantum Chem*., 2018, **118**, e25562.

36 J. C. Sancho-García, M. Moral, A. J. Perez-Jimenez, "Effect of Cyclic Topology on Charge-Transfer Properties of Organic Molecular Semiconductors: The Case of Cycloparaphenylene Molecules", *J. Phys. Chem. C*, 2016, **120**, 9104-9111.

37 S. Di Motta, E. Di Donato, F. Negri, G. Orlandi, D. Fazzi, C. Castiglioni, "Resistive Molecular Memories: Influence of Molecular Parameters on the Electrical Bistability", *J. Am. Chem. Soc.*, 2009, **131**, 6591.

38 E. Di Donato, R.P. Fornari, S. Di Motta, Y. Li, Z.H. Wang, F. Negri, "*n*-Type Charge Transport and Mobility of Fluorinated Perylene Bisimide Semiconductors", *J. Phys. Chem. B*, 2010, **114**, 5327.

39 S. Di Motta, M. Siracusa, F. Negri, "Structural and Thermal Effects on the Charge Transport of Core-Twisted Chlorinated Perylene Bisimide Semiconductors", *J. Phys. Chem. C*, 2011, **115**, 20754.

40 S. Canola, F. Negri, "Anisotropy of the *n*-type charge transport and thermal effects in crystals of a fluoro-alkylated naphthalene diimide: a computational investigation", *Phys. Chem. Chem. Phys.*, 2014, **16**, 21550-21558.

41 S. Canola, F. Negri, "Role of the HOMO‐1 Orbital on the *p*‐Type Charge Transport of the Fused-Ring Thienoacene DBTDT", *J. Phys. Chem. C*, 2015, **119**, 11499-11505.

42 S. Canola, C. Pecoraro, F. Negri, "Modeling *p*‐type charge transport in thienoacene analogs of pentacene", *Theor. Chem. Acc.*, 2016, **135**, 33.

43 S. Canola, C. Pecoraro, F. Negri, "Dimer and cluster approach for the evaluation of electronic couplings governing charge transport: Application to two pentacene polymorphs", *Chem. Phys.,* 2016, **478**, 130–138.

44 A. Troisi, "Charge Transport in High Mobility Molecular Semiconductors: Classical Models and New Theories", *Chem. Soc. Rev.*, 2011, **40**, 2347-2358.

45 A. Troisi, D. L. Cheung, "Modelling charge transport in organic semiconductors: from quantum dynamics to soft matter", *Phys. Chem. Chem. Phys.*, 2008, **10**, 5941–5952.

46 J.-L. Bredas, D. Beljonne, V. Coropceanu, J. Cornil, "Charge-Transfer and Energy-Transfer Processes in pi-Conjugated Oligomers and Polymers: A Molecular Picture", *Chem. Rev.*, 2004, **104**, 4971-5003.

47 V. Coropceanu, J. Cornil, D. A. da Silva, Y. Olivier, R. Silbey, J.-L. Bredas, "Charge Transport in Organic Semiconductors", *Chem. Rev.*, 2007, **107**, 926-952.

48 H. Oberhofer, K. Reuter, J. Blumberger, "Charge Transport in Molecular Materials: An Assessment of Computational Methods", *Chem. Rev.*, 2017, **117**, 10319-10357.

49 D. D. Méndez-Hernández, J. G. Gillmore, L. A. Montano, D. Gust, T. A. Moore, A. L. Moore, V. Mujica, "Building and testing correlations for the estimation of one-electron reduction potentials of a diverse set of organic molecules.", *J. Phys. Org. Chem.*, 2015, **28**, 320−328.

50 V. Barone, M. Cossi, "Quantum Calculation of Molecular Energies and Energy Gradients in Solution by a Conductor Solvent Model", *J. Phys. Chem. A*, 1998, **102**, 1995.

51 M. Cossi, N. Rega, G. Scalmani, V. Barone, "Energies, structures, and electronic properties of molecules in solution with the C-PCM solvation model", *J. Comput. Chem*., 2003, **24**, 669.

52 S. Grimme, J. Antony, S. Ehrlich, H. Krieg, "A consistent and accurate ab initio parametrization of density functional dispersion correction (DFT-D) for the 94 elements H-Pu", *J. Chem. Phys.*, 2010, **132**, 154104.

53 S. Grimme, S. Ehrlich, L. Goerigk, "Effect of the damping function in dispersion corrected density functional theory", *J. Comput. Chem.*, 2011, **32**, 1456.

54 Gaussian 09, Revision D.01, M. J Frisch, G. W. Trucks, H. B. Schlegel, G. E. Scuseria, M. A. Robb, J. R. Cheeseman, G. Scalmani, V. Barone, B. Mennucci, G. A. Petersson, et al. Gaussian, Inc., Wallingford CT, 2009.

55 F. Negri, G. Orlandi, "The resonance Raman spectra of 1,3,5-hexatriene and its deuterated derivatives: an ab initio re-investigation", *J. Chem. Phys.*, 1995, **103**, 2412-2419 .

View Article Online
DOI: 10.1039/C8CP06727A

56 F. Negri, M. Z. Zgierski, "Theoretical analysis of vibronic structure of absorption spectrum of fulvene", *J. Chem. Phys.*, 1995, **102**, 5165-5173.

57 B. Baumeier, J. Kirkpatrick, D. Andrienko, "Density-functional based determination of intermolecular charge transfer properties for large-scale morphologies", *Phys. Chem. Chem. Phys.*, 2010, **12**, 11103-11113.

58 A. Kubas, F. Hoffmann, A. Heck, H. Oberhofer, M. Elstner, J. Blumberger, "Electronic couplings for molecular charge transfer: Benchmarking CDFT, FODFT, and FODFTB against high-level ab initio calculations", *J. Chem. Phys.*, 2014, **140**, 104105.

59 A. Kubas, F. Gajdos, A. Heck, H. Oberhofer, M. Elstner, J. Blumberger, "Electronic couplings for molecular charge transfer: benchmarking CDFT, FODFT and FODFTB against high-level ab initio calculations. II", *Phys. Chem. Chem. Phys.*, 2015, **17**, 14342-14354.

60 A. Troisi, G. Orlandi, "The Hole Transfer in DNA: Calculation of Electron Coupling between Close Bases", *Chem. Phys. Lett.*, 2001, **344**, 509-518.

61 K. Senthilkumar, F. C. Grozema, F. M. Bickelhaupt, L. D. A. Siebbeles, "Charge transport in columnar stacked triphenylenes: Effects of conformational fluctuations on charge transfer integrals and site energies", *J. Chem. Phys.*, 2003, **119**, 9809-9817.

62 E. F. Valeev, V. Coropceanu, D. A. da Silva, S. Salman, J.-L. Bredas, "Effect of electronic polarization on charge transport parameters in molecular organic semiconductors", *J. Am. Chem. Soc.*, 2006, **128**, 9882–9886.

63 C. Schober, K. Reuter, H. Oberhofer, "Critical analysis of fragment-orbital DFT schemes for the calculation of electronic coupling values", *J. Chem. Phys.*, 2016, **144**, 054103.

64 H. Kim, T. Goodson III, P. M. Zimmerman, "Density Functional Physicality in Electronic Coupling Estimation: Benchmarks and Error Analysis", *J. Phys. Chem. Lett.*, 2017, **8**, 3242-3248.

65 J. Jortner, "Temperature dependent activation energy for electron transfer between biological molecules", *J. Chem. Phys.*, 1976, **64,** 4860–4867.

66 P. F. Barbara, T. J. Meyer, M. A. Ratner, "Contemporary Issues in Electron Transfer Research", *J. Phys. Chem.*, 1996, **100**, 13148-13168.

67 D. P. McMahon, A. Troisi, "Evaluation of the external reorganization energy of polyacenes", *J. Phys. Chem. Lett.*, 2010, **1**, 941–946.

68 E. Hennebicq, G. Pourtois, G. D. Scholes, L. M. Herz, D. M. Russell, C. Silva, S. Setayesh, A. C. Grimsdale, K. Müllen, J.-L. Brédas, "Exciton Migration in Rigid-Rod Conjugated Polymers: An Improved Förster Model", *J. Am. Chem. Soc.*, 2005, **127**, 4744–4762.

69 V. Stehr, R. F. Fink, C. Deibel, B. Engels, "Charge carrier mobilities in organic semiconductor crystals based on the spectral overlap", *J. Comput. Chem.*, 2016, **37**, 2146–2156.

70 V. Stehr, R. F. Fink, B. Engels, J. Pflaum, C. Deibel, "Singlet Exciton diffusion in organic crystals based on Marcus transfer rates", *J. Chem. Theory Comput.*, 2014, **10**, 1242–1255.

71 C. Sutton, J. S. Sears, V. Coropceanu, J.-L. Brédas, "Understanding the Density Functional Dependence of DFT-Calculated Electronic Couplings in Organic Semiconductors", *J. Phys. Chem. Lett.*, 2013, **4**, 919-924.

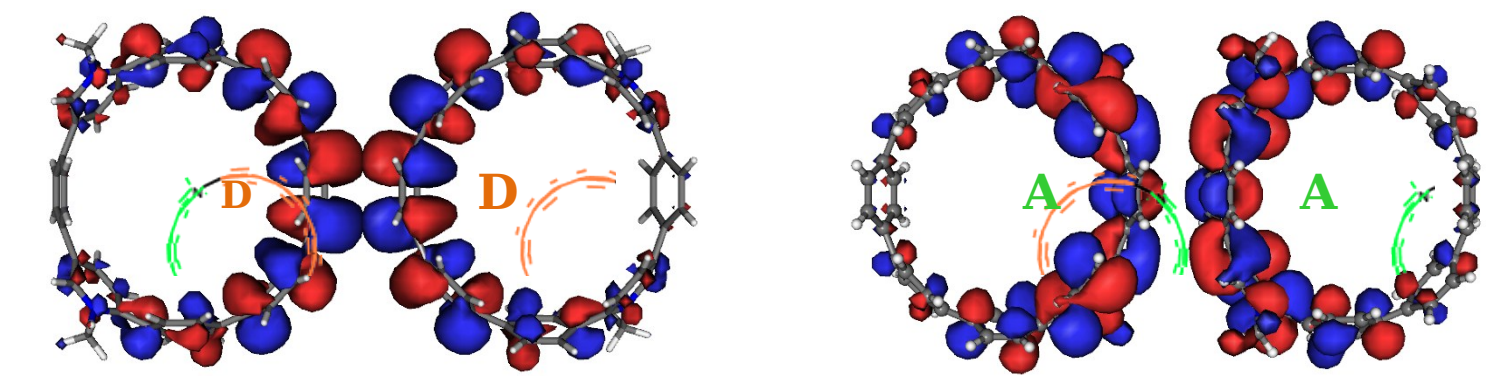

HOMO overlap
Large ***p*-type**
coupling

LUMO overlap
Large ***n*-type**
coupling